GEOPHYSICAL RESEARCH LETTERS, VOL. 36, L12603, doi:10.1029/2009GL038359, 2009

Diagnosis of vertical velocities in the upper ocean from high resolution sea surface height

P. Klein,[1] J. Isern-Fontanet,[2,3] G. Lapeyre,[4] G. Roullet,[1] E. Danioux,[1]
B. Chapron,[2] S. Le Gentil,[1] and H. Sasaki[5]

Received 26 March 2009; revised 6 May 2009; accepted 14 May 2009; published 18 June 2009.

[1] A surface Quasi-Geostrophy based (eSQG) method to diagnose the vertical velocity field from Sea Surface Height (SSH) is assessed using high resolution simulations. These simulations concern a turbulent eddy field with large Rossby numbers and energetic wind-driven motions. Results indicate that low-frequency vertical velocities (and also horizontal motions) can be reconstructed within a range of scales between 20 km and 400 km from the surface down to 500 m. The only information needed is a single high-resolution SSH snapshot and information on the large-scale vertical stratification. Inertial motions are naturally filtered because they do not contaminate SSH as we demonstrate. These results are encouraging and further strengthen previous studies using the eSQG method. They indicate that access to high resolution SSH may represent a major advance to retrieve horizontal and vertical fluxes of any tracer in the upper ocean. **Citation:** Klein, P., J. Isern-Fontanet, G. Lapeyre, G. Roullet, E. Danioux, B. Chapron, S. Le Gentil, and H. Sasaki (2009), Diagnosis of vertical velocities in the upper ocean from high resolution sea surface height, *Geophys. Res. Lett.*, *36*, L12603, doi:10.1029/2009GL038359.

1. Introduction

[2] Future space missions (using wide swath radar interferometer such as SWOT) aim to measure SSH at resolution as high as 10 km [*Fu and Ferrari*, 2008]. Such data should capture the surface signature of both mesoscale eddies ($\mathcal{O}$(100)km) and smaller structures with scales down to 10 km. Combined with recent theoretical results involving the SQG framework [*Lapeyre and Klein*, 2006] (hereafter LK06) and with some knowledge on the large-scale stratification, high resolution SSH may in addition allow to diagnose in the first 500 m the low-frequency (LF) motions, *including the vertical velocity field*. As such this would be a major advance compared with what allows the conventional radar altimetry. Attempts to diagnose the horizontal oceanic circulation, using LK06 results, from either the SSH or surface density have been already achieved in previous studies [*Isern-Fontanet et al.*, 2006, 2008]. But these studies involve small Rossby number (and therefore weak submesoscales) and very weak wind-driven motions, which corresponds to the assumptions which the LK06 diagnosis method is based on.

[3] The present study proposes to further assess the LK06 method in a more realistic situation, involving in particular a turbulent eddy field with large Rossby numbers (and therefore significant LF vertical motions) and energetic wind-driven near-inertial motions in the upper layers. For that purpose, we make use of a high resolution (2 km) simulation (described by *Klein et al.* [2008]) characterized by the presence of an energetic turbulent eddy field (the Rossby number is close to 0.3 near the surface) and of an active mixed-layer (ML) forced by realistic high-frequency winds [*Klein et al.*, 2004]. The resulting vertical velocity field in the first 500 m includes an energetic near-inertial component and a component related to the mesoscale turbulent eddy field. This simulation is used as a testbed to further assess the LK06 method and in particular to reveal whether the LF 3D circulation associated with the mesoscale and submesoscale structures can be retrieved from high resolution SSH. The next section briefly reviews the LK06 diagnosis method. Section 3 presents the numerical solutions used. Section 4 compares the diagnosed 3-D oceanic circulation with the one observed with a focus on the vertical velocity. Conclusions are offered in the last section.

2. Method

[4] LK06 showed that, for baroclinic flows, potential vorticity (PV) anomalies in the ocean interior are correlated to the surface PV (or surface buoyancy) anomalies. Using this property and the invertibility principle of PV [*Hoskins et al.*, 1985], they proposed a method to diagnose the 3D dynamics in the upper ocean from either the SSH or the surface buoyancy. This method, called the ''effective' SQG (eSQG) method (since it is based on the SQG dynamics [*Held et al.*, 1995]), allows to get the geostrophic streamfunction (ψ) at any depth from the SSH (η), using

$$\widehat{\psi}(\mathbf{k},z) = \frac{g}{f}\widehat{\eta}(\mathbf{k})\exp\left(\frac{N_0}{f}kz\right), \tag{1}$$

where $\widehat{(.)}$ stands for the horizontal Fourier transform, $\mathbf{k} = (k_x, k_y)$ is the wavenumber vector and $k = |\mathbf{k}|$ its modulus. f is the Coriolis frequency, g the gravity constant. N_0 is an ''effective'' Brunt-Väissälä frequency that takes into account the contribution of the interior PV [see LK06; *Isern-Fontanet et al.*, 2008]. Then, horizontal motions and relative vorticity (ζ) are diagnosed from geostrophy and buoyancy (b) from hydrostaticity. Vertical motions (w) are retrieved from the buoyancy equations (at the surface and at

[1]Laboratoire de Physique des Océans, IFREMER, UBO, IRD, CNRS, Plouzané, France.
[2]Laboratoire d'Océanographie spatiale, IFREMER, Plouzané, France.
[3]Institut Català de Ciències del Clima, Barcelona, Spain.
[4]Laboratoire de Météorologie Dynamique, IPSL, ENS, CNRS, Paris, France.
[5]Earth Simulator Center, JAMSTEC, Yokohama, Japan.

0094-8276/09/2009GL038359$05.00

depth) [*Hakim et al.*, 2002], which is an alternative to the classical Omega equation [*Hoskins et al.*, 1985]. The resulting diagnostic relations are (see LK06)

$$\widehat{b}(\mathbf{k},z) = \frac{N_0 k}{c}\widehat{\psi}(\mathbf{k},z), \tag{2}$$

$$\widehat{\zeta}(\mathbf{k},z) = -k^2\widehat{\psi}(\mathbf{k},z), \tag{3}$$

$$\widehat{w}(\mathbf{k},z) = -\frac{c^2}{N_0^2}\left[-\widehat{J(\psi_s,b_s)}\exp\left(\frac{N_0}{f}kz\right) + \widehat{J(\psi,b)}\right], \tag{4}$$

with $J(A, B) \equiv \partial_x A \partial_y B - \partial_x B \partial_y A$. Subscript "s" refers to surface values. The assumptions necessary for deriving these equations restrict their applicability to frequencies smaller than the inertial frequency and scales smaller than 400 km. Note that equation (1) indicates a strong phase relationship between surface and interior dynamical quantities down to a depth that depends on the wavenumber.

[5] This method requires to fix two constants, N_0 and c. N_0 is usually derived from existing observations of the large-scale density field [e.g., *Isern-Fontanet et al.*, 2008], and c is usually estimated comparing surface kinetic energy with independent observations [e.g., *Isern-Fontanet et al.*, 2006, 2008]. However, since the full velocity field was available in the present study we have estimated N_0 so as to match the observed shape of the vertical profile of the enstrophy variance and c from the maximum amplitude of the observed w. For the simulation used in the present study, the resulting values are $N_0/f = 30$ and $c = 1.15$.

3. Numerical Solutions

[6] The numerical simulation used (fully described by *Klein et al.* [2008]) has been performed with a Primitive Equation code and concerns a fully turbulent flow field in a zonal β-plane channel centered at 45°N with a size of 1000 km × 2000 km and a depth of 4000 m. The resolution is 2 km in the horizontal and 100 levels on the vertical. The vertical profile of the mean Brunt-Väisälä frequency (not shown) involves a main thermocline located at a depth around 600 m that corresponds to a first Rossby radius of deformation of approximately 30 km. The mesoscale eddy turbulence is forced by using a relaxation to a basic state that corresponds to a large-scale meridional density gradient [see *Klein et al.*, 2008]. An active ML with a depth of 80 m, forced by a realistic time series of high-frequency winds (described by *Klein et al.* [2004]) and surface heat fluxes, caps a seasonal thermocline whose thickness is about 40 m.

[7] The velocity wavenumber spectrum near the surface (not shown) has a peak at 300 km and a slope close to k^{-2} [see *Capet et al.*, 2008; *Klein et al.*, 2008]. Below 500 m, the velocity wavenumber spectrum [see *Klein et al.*, 2008] has still a peak at 300 km but its slope is steeper (in k^{-3}). Root Mean Square (RMS) value of the relative vorticity within the eddy field is maximum at the surface ($0.32\,f$) and decreases down to $0.24\,f$ at 200 m and $0.14\,f$ at 500 m. Meridional section of the relative vorticity and vertical velocity fields (Figure 1a) emphasizes the signature of the ML. The vertical velocity field displays significant amplitudes within the ML but also well below the ML (Figure 1a). This field is small-scale at 200 m (its wavenumber spectrum (not shown) has a peak at 60 km and a slope in k^{-2}). At this depth it is strongly related to the small-scale vorticity structures through frontogenesis. Below 500 m the vertical velocity field is dominated by larger scales (its wavenumber spectrum (not shown) has a peak at 150 km and a slope in k^{-3}). The RMS value of the instantaneous vertical velocity (red curve on Figure 1b) reveals a subsurface maximum around 300 m equal to 16 m/day and a secondary maximum near the bottom of the ML. After filtering the inertial frequency, the resulting LF part of the vertical velocity (blue curve on Figure 1b) displays a maximum amplitude smaller by a factor 1.5. The difference between the two curves is entirely explained by the near-inertial motions, which highlights their energetic contribution. The LF part is explained by the contribution of the mesoscale eddy field and by the Ekman pumping.

[8] One important characteristic revealed by this simulation is the absence of an inertial peak in the frequency spectrum of the SSH (green curve on Figure 1c) whereas the spectrum of the observed surface horizontal motions displays a significant peak at this frequency (red curve on Figure 1c). A budget analysis of the SSH equation actually reveals that there is a strong compensation between the advective terms (that have a significant inertial signature) and the vertical velocity near the surface at the inertial peak (a full explanation will be given in a subsequent paper).

[9] An additional characteristic is the very good spectral correlation between the surface vorticity deduced from the SSH and the instantaneous vorticity observed in the interior (Figure 2a). A similar spectral correlation is observed between the surface and interior density. Such correlation indicates, for a given wavelength, a strong phase relationship between the surface and interior for these quantities down to a depth that depends on this wavelength. Thus scales of the order of $\mathcal{O}$(50)km are correlated down to a depth not larger than 400 m, but scales of $\mathcal{O}$(200)km are correlated down to 1000 m. Such spectral correlation has been observed in the realistic North Atlantic simulation used by *Isern-Fontanet et al.* [2008], for a range of scales from 500 km down to 30 km. It is also reported by Cabanes et al. (submitted manuscript, 2009) and *Qiu and Chen* [2005] from the analysis of altimeter data and subsurface Argo floats data that capture mesoscales. The depth dependence on the wavenumber revealed by Figure 2a appears to be close to the vertical decay scale law expressed in equation (1) as illustrated by the black curve. Figure 2a further indicates that this vertical decay scale law works well for scales larger than 20 km but is no more valid for smaller scales because of the presence of the ML. On the other hand Figure 2b that shows the correlation between surface geostrophic and observed motions emphasizes the dominance of the geostrophic contribution (deduced from SSH) for scales larger than 20 km. For smaller scales this correlation quickly decreases indicating that the energetic wind-driven contribution to horizontal motions becomes significant. This indicates that the specific ML dynamics is mostly captured by scales smaller than 20 km.

4. Diagnosis Results

[10] Since near-inertial motions have no signature on the SSH, this quantity has been used to diagnose the 3D

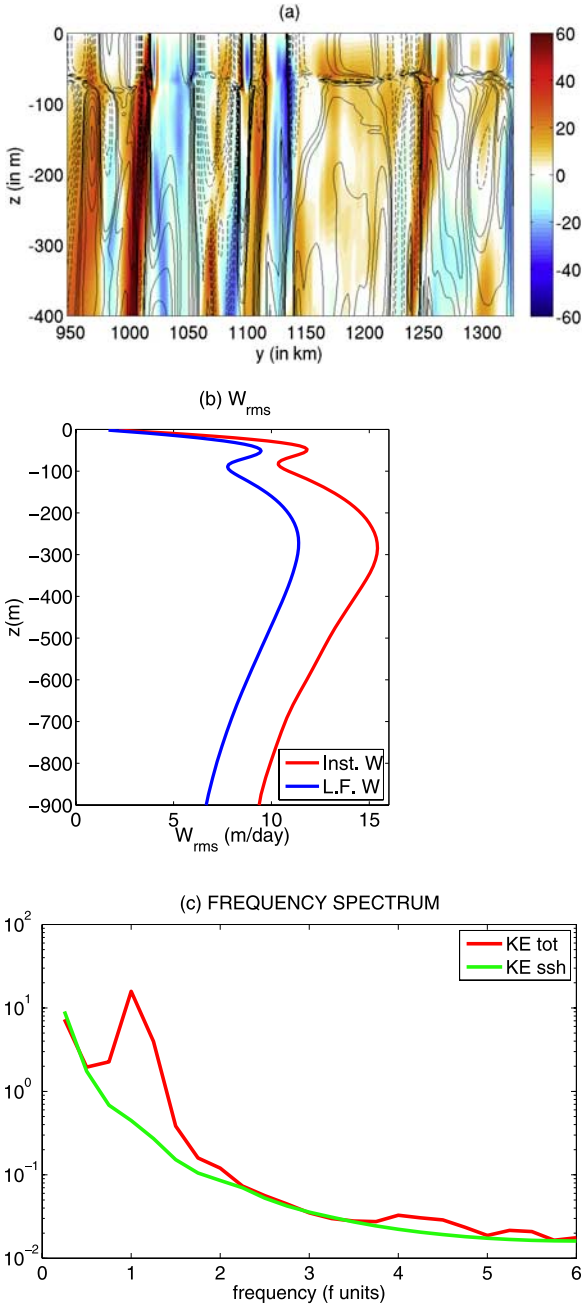

Figure 1. (a) Snapshot of a vertical section of w (color) and of the relative vorticity (in contours). Units for w are in m/day and relative vorticity contour intervals correspond to $4 \times 10^{-6}\mathrm{s}^{-1}$. (b) Vertical profiles of the rms value of the instantaneous vertical velocity (red) and of the vertical velocity averaged over an inertial period (blue). (c) Frequency spectrum of the surface kinetic energy deduced from u and v (red line) and from the SSH using the geostrophic approximation (green line).

circulation using the eSQG method. As indicated before, this method is valid only for LF motions with scales smaller than $\mathcal{O}(400$ km). Scales smaller than 20 km are not considered since they are affected by the wind-driven ML dynamics for which the method does not work. Consequently the SSH data used are those obtained from the observed SSH by applying a high-pass filter of 400 km and a low-pass filter of 20 km. Then the streamfunction, relative vorticity, buoyancy and, vertical velocity at any depth have been diagnosed from equation (1) to equation (4). Classical 2D Fourier transforms assuming double periodic conditions (the channel domain is periodic in the zonal direction and has a width twice larger than the width of the turbulent flow) are used to go to the spectral space and back to physical space. The diagnosed fields are then compared to the observed ones, averaged over an inertial period to get their LF part and after applying to them the same spatial filters. An example of such observed and diagnosed fields at 200 m are shown on Figures 3a and 3b. A remarkable visual coincidence is exhibited between both fields down to scales as small as 20 km.

[11] To quantify the quality of the diagnosis at any depth, we have computed the correlation between the diagnosed fields and the LF part of the observed fields, as well as the RMS amplitudes of both fields. We focus on the 3D motions and more specifically on the relative vorticity and vertical velocity. Results indicate that the correlation of the diagnosed vertical velocity with the LF observed one is close to 0.7 between 100 m and 1000 m (Figure 3c). The vertical profile of the w_{rms} well compares with the observed one at any depth down to 1000 m (Figure 3d). The vorticity correlation decreases monotonically with depth, from 0.9 near the surface to 0.7 at 500 m (Figure 3c). Its further decrease below 500 m is explained by the contribution of

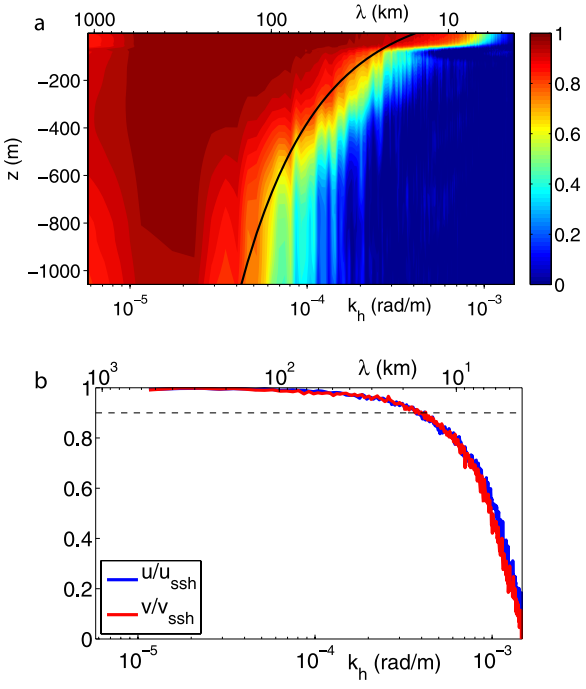

Figure 2. (a) Spectral correlation between the surface vorticity and the vorticity at depth. The black curve corresponds to $\exp(\frac{N_0}{f}\ k\ (z - z_o)) = 0.85$ with $z_o = -120$ m. It is the depth dependence on the wavenumber k, using equation (1), of the correlation amplitude equal to 0.85. (b) Spectral correlation between the observed surface velocity (u and v) and the surface velocity deduced from the SSH using the geostrophic approximation (u_{ssh} and v_{ssh}).

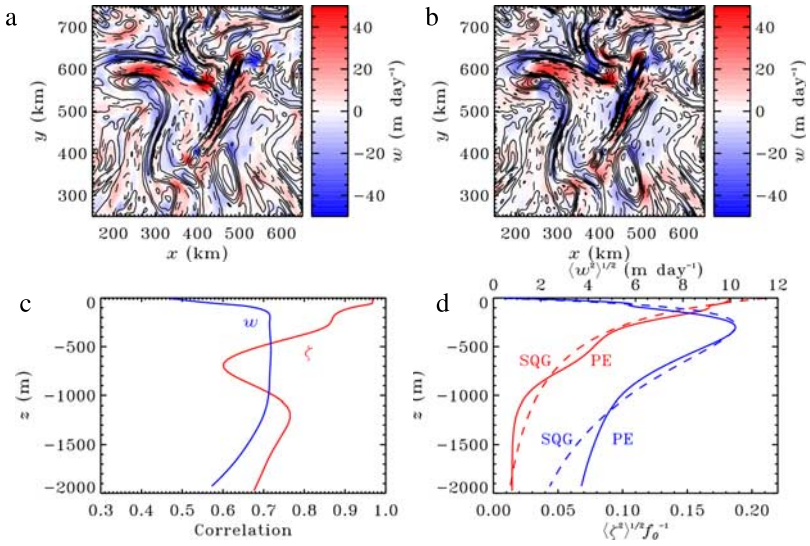

Figure 3. (a) Observed LF vertical velocity (in colors) and relative vorticity (contours) at 200 m. (b) eSQG reconstructed vertical velocities (in colors) and relative vorticity (contours) at 200 m. Units for LF w are in m/day and relative vorticity contour intervals correspond to $4 \times 10^{-6}\mathrm{s}^{-1}$. (c) Correlation between observed and eSQG reconstructed vertical velocities (blue line) and relative vorticity (red line). (d) Vertical velocities RMS (blue) and relative vorticity RMS (red) observed in the PE simulation (solid line) and reconstructed using eSQG (dashed line).

the small scales that is still non-negligible there (the vorticity spectrum has a k^{-1} slope at 600 m): these scales at these depths are missed by the eSQG method because of the exponential form. On the other hand the small-scale contribution to the w-field is negligible at these depths (see previous section) which explains the better correlation for this field. As expected, results within the ML are not so good. Note that the secondary maximum of the vertical velocity (near the bottom of the ML) present on the blue curve of Figure 1b becomes much weaker after the spatial filtering (solid blue curve on Figure 3d) and is absent in the diagnosed field (dashed blue curve on Figure 3d). This maximum is very likely due to the ML dynamics and Ekman pumping (not taken into account in the eSQG method). The vorticity field seems to be less affected in the ML but its variance is overestimated. Thus, because of these deficiencies, we can consider that the diagnosis is correct only from the ML base down to 500 m.

5. Conclusion

[12] Diagnosis capabilities of the eSQG method have been further explored in presence of a mesoscale eddy field with large Rossby numbers and an active ML forced by high frequency winds. Results further strengthen previous studies using the eSQG method. They reveal that, despite the presence of energetic near-inertial motions, a snapshot of high resolution SSH allows reconstruction of the LF motions, including the vertical velocities, but only for scales between 400 km and 20 km and for depths between the ML base and 500 m. As such they highlight the potential of high-resolution SSH to assess the LF horizontal and vertical fluxes of momentum and tracers in the upper ocean driven by mesoscale eddy dynamics. Some work has still to be done to improve this simple diagnosis method. This includes its testing in a broader range of mesoscale eddy and ML regimes and its improvement to diagnose the specific ML dynamics. Furthermore a more appropriate estimation of the two constants, N_0 and c, should be searched for. One approach would be using the sea surface temperature, climatological values of the vertical stratification (as attempted by *Isern-Fontanet et al.* [2006, 2008] and *Klein et al.* [2008]) and/or the existing Argo float data. The large-scale density field retrieved from these data can indeed be used to get information of the vertical coherence of PV anomalies which subsequently allows to get an estimation of N_0 (see LK06 expressions (12) and (26) to (29)).

[13] **Acknowledgments.** This work is supported by IFREMER, CNRS (FRANCE), the Agence Nationale pour la Recherche (contract ANR-05-CIGC-010). Numerical simulations reported here were done at IDRIS (France) and on the Earth Simulator (Yokohama, Japan) through a M.O.U. signed between IFREMER, CNRS and JAMSTEC. We thank Xavier Capet for thoughtful comments. JIF has been supported by a Marie Curie IntraEuropen (EIF) grant (041476-OCEAN3D). We thank both reviewers for their insightful comments.

References

Capet, X., J. C. McWilliams, M. Molemaker, and A. Shchepetkin (2008), Mesoscale to submesoscale transition in the california current system. Part 1: Flow structure and eddy flux, *J. Phys. Oceanogr.*, *38*, 29–43.

Fu, L.-L., and R. Ferrari (2008), Observing oceanic submesoscale processes from space, *Eos Trans. AGU*, *89*(48), doi:10.1029/2008EO480003.

Hakim, G. J., C. Snyder, and D. J. Muraki (2002), A new surface model for cyclone-anticyclone asymmetry, *J. Atmos. Sci.*, *59*, 2405–2420.

Held, I. M., R. T. Pierrehumbert, S. T. Garner, and K. L. Swanson (1995), Surface quasi-geostrophic dynamics, *J. Fluid Mech.*, *282*, 1–20.

Hoskins, B. J., M. E. McIntyre, and A. W. Robertson (1985), On the use and significance of isentropic potential vorticity maps, *Q. J. R. Meteorol. Soc.*, *111*, 877–946.

Isern-Fontanet, J., B. Chapron, G. Lapeyre, and P. Klein (2006), Potential use of microwave sea surface temperatures for the estimation of ocean currents, *Geophys. Res. Lett.*, *33*, L24608, doi:10.1029/2006GL027801.

Isern-Fontanet, J., G. Lapeyre, P. Klein, B. Chapron, and M. W. Hecht (2008), Three-dimensional reconstruction of oceanic mesoscale currents

from surface information, *J. Geophys. Res.*, *113*, C09005, doi:10.1029/2007JC004692.

Klein, P., B. Hua, G. Lapeyre, X. Capet, S. L. Gentil, and H. Sasaki (2008), Upper ocean turbulence from high 3-D resolution simulations, *J. Phys. Oceanogr.*, *38*, 1748–1763.

Klein, P., G. Lapeyre, and W. G. Large (2004), Wind ringing of the ocean in presence of mesoscale eddies, *Geophys. Res. Lett.*, *31*, L15306, doi:10.1029/2004GL020274.

Lapeyre, G., and P. Klein (2006), Dynamics of the upper oceanic layers in terms of surface quasigeostrophy theory, *J. Phys. Oceanogr.*, *36*, 165–176.

Qiu, B., and S. Chen (2005), Eddy-induced heat transport in the subtropical North Pacific from argo, tmi and altimetry measurements, *J. Phys. Oceanogr.*, *35*, 458–473.

B. Chapron and J. Isern-Fontanet, Laboratoire d'Océanographie Spatiale, IFREMER, BP 70, F-29280 Plouzané CEDEX, France.

E. Danioux, P. Klein, S. Le Gentil, and G. Roullet, Laboratoire de Physique des Océans, IFREMER, UBO, IRD, CNRS, BP 70, F-29280 Plouzané CEDEX, France. (patrice.klein@ifremer.fr)

G. Lapeyre, Laboratoire de Météorologie Dynamique, IPSL, ENS, CNRS, 24 Rue Lhomond, F-75005 Paris CEDEX, France.

H. Sasaki, Earth Simulator Center, JAMSTEC, 3173-25 Showa-machi, Kanazawa-ku, Yokohama, Kanagawa 236-0001, Japan.